A New Approach to Partial Discharge Detection Under DC Voltage: Application to Different Materials

Pietro Romano,[1] Antonino Imburgia,[1] Giuseppe Rizzo,[1] Guido Ala,[1] and Roberto Candela[2]

[1]L.E.PR.E. HV Laboratory, Department of Engineering, Palermo University, Palermo, 90128, Italy; and [2]Prysmian Electronics Srl, Palermo, Italy

Key words: HVDC, partial discharge, DC measurements, testing method, pattern recognition, discharge phenomena

Usability of a new Direct Current Periodic waveform for partial discharge qualification in HVDC systems is exemplified by tests performed on different materials.

Introduction

In the recent years the development of high voltage direct current (HVDC) power transmission systems has revealed issues related to the assessment of their reliability [1]–[3]. In particular, due to the characteristics of the phenomenon, there is no consolidated method for measuring partial discharges (PDs) to identify insulation defects under DC stresses [4]. Despite the same phenomenon occurring under AC stress, where the standard IEC 60270 is used [5], no technical standards have been developed for DC. In addition, with the same applied voltage magnitude, under constant voltage supply, the PD repetition rate is lower than under alternating voltage [6], [7]. In other words, to identify a defect within the insulation, the DC voltage stress must be applied for a longer time than that under AC to gain statistics. Moreover, to identify the defect type, the phase-resolved-partial-discharge (PRPD) pattern, which is helpful to identify the defect type, cannot be created under DC stress [8]–[11]. This is due to the constant shape of the DC stress, which does not allow a phase value be assigned to the discharge event but only the time of appearance from $t = 0$. To overcome these main problems related to the PD measurements under DC stress, some authors have proposed new techniques mainly based on a DC voltage with superimposed periodic waveforms or ripples [12]–[16]. Furthermore, some IEC standards and recommendations of IEEE and CIGRÈ have proposed test methods for HVDC extruded cables and accessories adopting PD measurement techniques suitable for AC [17]–[20]. This solution could give good results in terms of research of defects generated during the fabrication process. However, under DC stress, the presence of space charge phenomena strongly influences the electric field distribution inside the dielectric and the discharge conditions dramatically change compared with AC [8]. For this reason, the application of an AC wave shape could lead to approximate or incorrect results. With the aim to investigate the differences in PD measurements under AC and DC, a new waveform has been proposed by the authors in a previous work [21]. The new waveform is named "direct current periodic" (DCP) and consists of both a sinusoidal and a constant part for a period. With the use of the DCP, it is possible to stress the specimen with the same effect as a pure DC voltage and detect PDs as with an AC waveform. Moreover, thanks to the sinusoidal part of the DCP waveform, it is possible to obtain the PD probe synchronization and therefore the origin of the PRDP pattern [21].

In the previous article [21], after describing the DCP waveform and the measurement setup, PD tests were performed on a Kapton specimen. The findings of that research show some interesting results in terms of partial discharge inception voltage (PDIV) and repetition rate (PDRR). In particular, the PDIV results follow a second order polynomial law, depending on the parameter δ, going from 2.0 kV peak value in AC to 14 kV in DC. At the same time, with the same variation's law, the PDRR decreases from 66 PD/second in AC to 0.084 PD/second in DC. Another finding, under the proposed DCP waveform, is the possibility to identify discharges in defects and discriminate simultaneous multiple phenomena as in AC.

This work continues the investigation in [21] by extending the DCP method to other polymeric materials, namely cross-linked polyethylene (XLPE), polyethylene terephthalate (PET), and mineral oil mass impregnated (M.I.) paper. Measurements are also repeated again on Kapton specimens. Results confirm that polymeric materials have the same behavior, whereas M.I. paper differs slightly in terms of PDIV.

The DC Periodic Stress

The DCP waveform was developed and reported in detail in [21]. Here, a brief description is given. The DCP waveform is mathematically described in Equation (1), and its shape, with

 0883-7554/21/©2021/IEEE

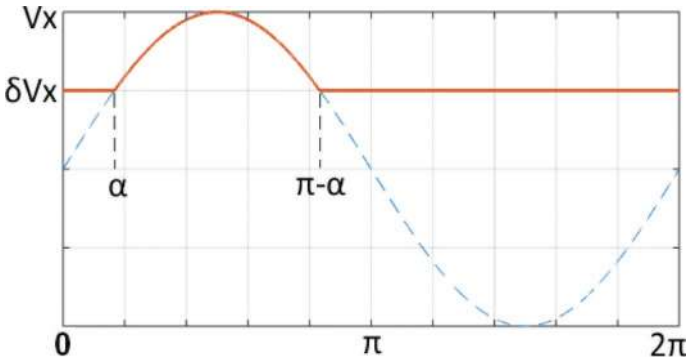

Figure 1. Direct current periodic waveform in positive polarity.

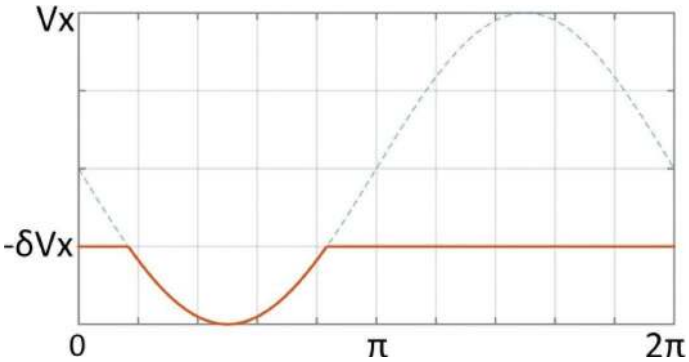

Figure 2. Direct current periodic waveform in negative polarity.

positive and negative polarity, is shown in Figures 1 and 2, respectively. The introduction of the negative polarity in this work is due to the interest in reversal polarity phenomena in HVDC systems, even if in this paper tests with polarity shifts are not included [22]. The DCP waveform follows a sinusoidal law from α to $\pi - \alpha$ and it is constant over the remainder of the period. Considering that δ can assume values from −1 to +1, the parameter δV_x takes values in the range $\pm V_x$. When $\delta = 0$, also $\alpha = 0$ and the waveform is sinusoidal for half a period and zero for the rest. When $\delta = \pm 1$, the waveform coincides with pure DC with $\pm V_x$ amplitude. Therefore, by varying δ, the applied waveform assumes transient values from half AC wave to DC. Furthermore, for $\delta = \pm 0.625$ the RMS value of DCP coincides with the RMS value of an AC sinusoidal voltage with $\pm V_x$ amplitude.

$$v(t) = \begin{cases} V_x \sin(\omega t) & \text{for } \alpha \le \omega t \le \pi - \alpha \\ \delta V_x & \text{for } 0 \le \omega t < \alpha, \quad \pi - \alpha < \omega t \le 2\pi \end{cases} \tag{1}$$

The sinusoidal component of the test voltage plays an important role in the proposed PD testing method, because it not only determines the triggering moments of the recording of measurement signals, but also significantly affects the activity of PD in the tested insulation systems (model samples).

Another fundamental aspect to describe is the comparison between DCP and DC in terms of space charge accumulation and its influence on the occurrence of PDs. The evaluation of the charge accumulated at the interface between air and dielectric plays an important role in the establishment of conditions enhancing PDs. For this reason, the charge accumulated near the interface in the case of a periodic DC source has been compared with that occurring in the case of a pure DC source. By combining the current continuity equation, Ohm's law for the current density and Gauss' law for the volumetric charge density, the space charge density can be evaluated through the following equations:

$$J = \sigma E, \tag{2}$$

$$\nabla \cdot J = -\partial \rho_C / \partial t, \tag{3}$$

$$\nabla \cdot (\varepsilon_0 \varepsilon_r E) = \rho_C, \tag{4}$$

$$-\nabla V = E, \tag{5}$$

where E is the electric field, ε_0 is the vacuum permittivity, ε_r is the relative permittivity and ρ_C is the free volumetric charge density. Equations (2) to (5) have been numerically solved by applying the finite volumes method (FVM) to a one-dimensional geometry that models the flat sample. Therefore, the charge accumulation at the interfaces and within the dielectric has been evaluated by means of a conductivity model. This approach does not take into account the contribution of space charge phenomena related to the lattice structure of the dielectric material, namely the presence of impurities, electron trapping and detrapping. However, these phenomena play a non-relevant role under the relatively small electric fields applied in this study.

Equations (2) to (5) have been solved iteratively in the time domain by means of a code implemented in Matlab®. First, the space charge distribution is set equal to zero at the initial time step; then, the electric field distribution is calculated by means of the Equations (4) and (5). The current density is therefore obtained by Equation (2) and considering Schottky injection at the interfaces as time dependent boundary conditions. Once the current distribution has been calculated, the increase in the space charge density can be evaluated in each calculation volume. The space charge distribution is then introduced into Equation (4) and another iteration cycle begins.

The interface thickness was set equal to zero; therefore, the output value of ρ is dependent on the chosen spatial interval. However, the product between the spatial interval in the direction of the electric field and ρ returns the surface charge density. A simulation has been carried out for an air-XLPE sample with a peak voltage of the AC source equal to 5 kV and δ equal to 0.6. Then, the resulting surface charge density was compared with the calculated one by considering a pure DC source equal to 3 kV. In Figure 3, the comparison between the resulting surface charge densities versus time is shown. The accumulation of charge at the interface depends on the RMS value of the applied voltage. With reference to the above-mentioned periodic DC voltage, the asymptotic value of the surface charge density is equal to that occurring if a 3.4-kV DC voltage is applied to the sample.

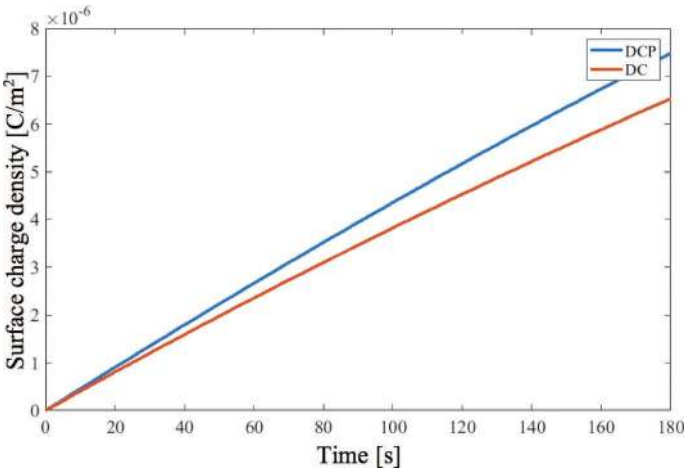

Figure 3. Accumulated surface charge density for 5-kV direct current periodic (DCP) with δ = 0.6 (blue line) and 3-kV DC (red line).

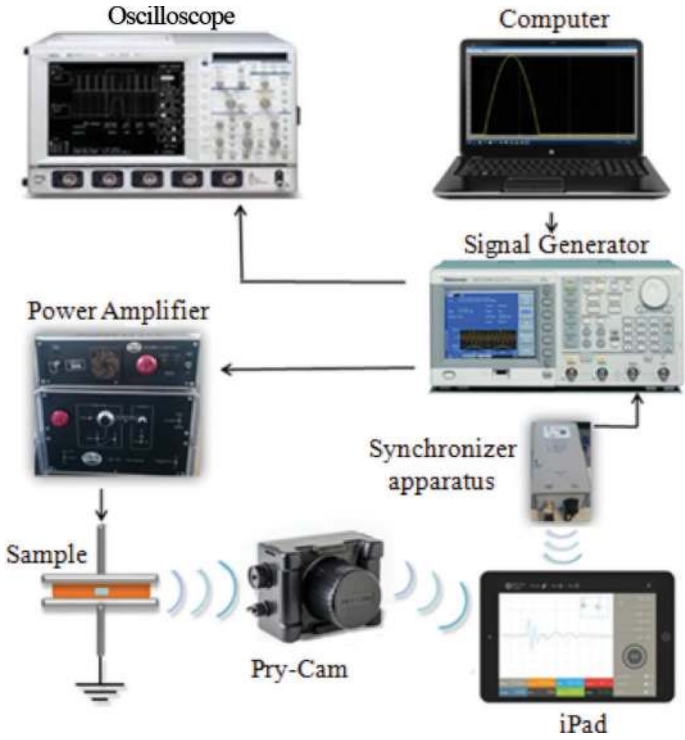

Figure 4. Experimental setup.

Experimental Setup and Specimens Under Test

The measurement setup is shown in Figure 4. The DCP waveform is generated by a code implemented in Matlab® with positive or negative polarity and different δ values. After its generation, the DCP waveform is sent to a signal generator whose maximum output voltage magnitude is equal to ±10 V. To amplify the DCP voltage signal up to 1,000 times, a Trek power amplifier is used. Finally, the amplifier output signal is applied to the specimen under test. To detect the PD phenomena, the Pry-Cam portable antenna sensor is employed [20]. A synchronizer apparatus is connected to the TTL port of the function generator to read the generated DCP waveform frequency and synchronize the PD probe to create the PRPD pattern. The antenna sensor is also directly capable of synchronizing with the DCP waveform. The digital system connects via Wi-Fi to an iPad for remote control and display of the acquired signals. The PRPD pattern, the time domain trend, and the fast Fourier transform (FFT) of all acquired PD signals can be displayed and stored [20].

Test samples of different materials are made of two layers of the same dielectric material. In the upper layer (the one in contact with the high voltage electrode), a hole 300 µm in diameter is made to create an air void defect and enhance internal discharges, as shown in Figure 5. The two-layer asymmetrical configuration has been chosen instead of the more classic three-layer to reduce the PDIV and partially exceed the limit of 10 kV of the power amplifier.

With the aim of investigating the behavior of materials subjected to DCP stress, and assess any differences with respect to Kapton's behavior, another two polymeric materials and one mass impregnated paper have been selected. Cross-linked polyethylene, XLPE, and mass-impregnated paper are mainly used in the cable industry. In addition, poly(ethylene terephthalate), PET, is used in various electrical applications.

For each material, the layer thickness, d; the dielectric relative permittivity, ε_r; and the resistivity, ρ, are reported in Table 1. An additional lower solid layer has been added for M.I. paper only, to avoid breakdowns occurring with a specimen of only two layers.

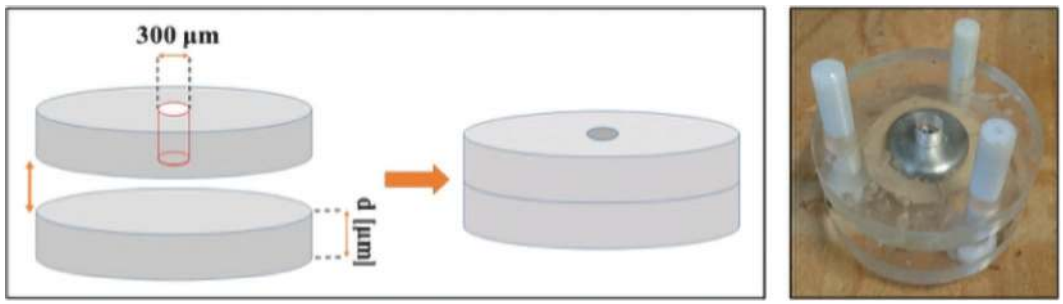

Figure 5. Specimen under test composed of two dielectric layers with thickness d. A hole is made in one foil to obtain internal partial discharges.

Table 1. Dielectric material properties

Material	d (μm)	ε_r	ρ (Ωm)
Kapton	127	2.24	$1 \cdot 10^{15}$
Cross-linked polyethylene (XLPE)	90	2.23	$1 \cdot 10^{11}$
Polyethylene terephthalate (PET)	110	3	$1 \cdot 10^{11}$
Mineral oil mass impregnated (M.I.) paper	150	4.5	$4.7 \cdot 10^{11}$
Air	2	1	$2 \cdot 10^{16}$

[1] d = layer thickness; ε_r = dielectric relative permittivity; and ρ = resistivity.
[2] Air dimension d was always the same of the adopted solid material.

Test Procedure and Experimental Results

The specimens listed in Table 1 were subjected to both 50 Hz AC and DCP waveforms. All measurements were typically performed within a few minutes of voltage application. First, as a reference measurement, the AC stress was applied and the PDIV value as well as the PRPD patterns were recorded. Then, the same procedure was carried out by applying the DCP stress. In this case, the PD acquisitions were made for different δ values (from 0 to 1 with a spacing of 0.2) and for both voltage polarities. For each PD test, after detecting the PD inception voltage, the voltage was increased at 0.5 kV/second from zero to the value at which the discharges were repetitive; the acquisition was stopped at stabilized PDRR values. After each PD measurement, each specimen was short-circuited to remove the accumulated charges, which otherwise would have compromised subsequent measurements.

In the next paragraphs, the experimental results for all specimens are reported in detail.

Kapton

Measurements of PDs occurring in Kapton specimens have been repeated to confirm the results obtained in the previous paper [21]. As specified in the introduction part of the paragraph, first, the AC measurements were done as starting reference parameters. Then, the DCP tests with increasing values of δ for both polarities were performed.

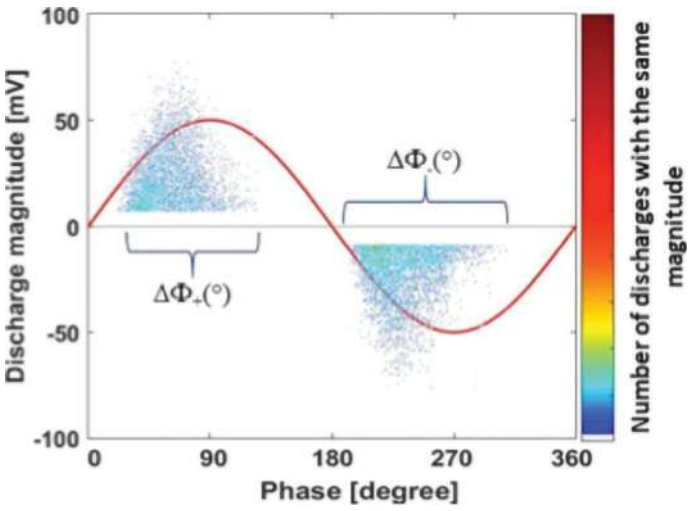

Figure 6. Phase-resolved partial discharge pattern under 1.4-kV peak value 50-Hz AC stress. $\Delta\Phi_+$ and $\Delta\Phi_-$ are the width of the spectrum for positive and negative partial discharges, respectively.

Figure 7. Time domain partial discharge pulse detected under AC stress.

- **AC test.** PD measurement under AC voltage shows a standard internal cavity behavior with high PD amplitude variability and left inception phase angle shift with voltage increase. The PDIV has been detected at 1.4 kV peak value, and the corresponding PRPD pattern is shown in Figure 6. The brackets $\Delta\Phi_+$ and $\Delta\Phi_-$ represent the widths of the spectrum for positive and negative PDs, respectively.

To verify that the AC waveform provides the same PD signal as that due to a DCP stress, in terms of pulse time and frequency domain trend, an acquired PD pulse and its frequency spectrum are presented in Figures 7 and 8, respectively. The pulse shape in Figure 7 has a typical second order response, and the first two oscillations last about 130 nanoseconds. In the frequency spectrum of Figure 8, the most dominant frequency is about 5 MHz.

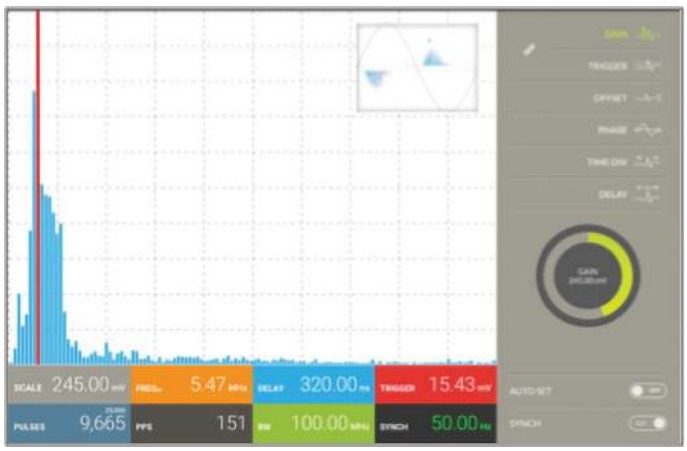

Figure 8. Frequency spectrum of the partial discharge pulse under AC stress.

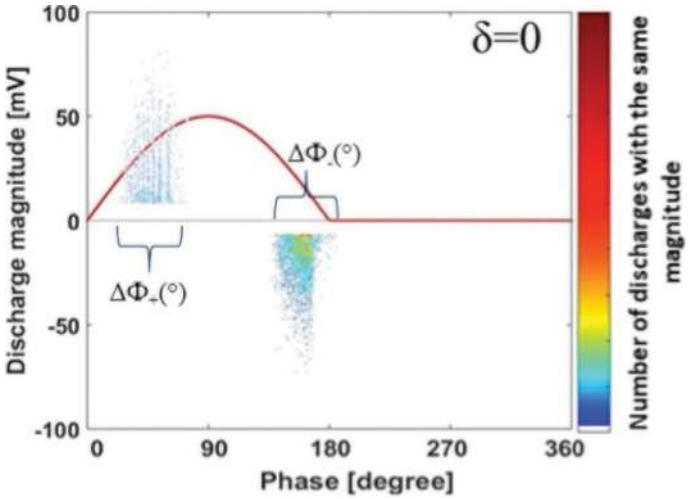

Figure 9. Phase-resolved partial discharge pattern under 2.2-kV peak value 50-Hz direct current periodic positive polarity with $\delta = 0$. $\Delta\Phi_+$ and $\Delta\Phi_-$ are the width of the spectrum for positive and negative partial discharges, respectively.

- **DCP tests.** By applying the DCP waveform with positive polarity and $\delta = 0$, the PD inception occurs at 2.2 kV, and the obtained PRPD pattern is shown in Figure 9.

By making a comparison between the PRPD pattern of the sinusoidal stress of Figure 6 and the PRPD pattern of the DCP, some conclusions can be made. Some of these have already been discussed in the previous paper as the presence of both negative and positive discharges. In particular, the pattern of Figure 9 shows a reduction in the width of the discharge pulse phase; thus, the values of $\Delta\Phi_+$ and $\Delta\Phi_-$ are lower. Furthermore, positive discharges stop before the dv/dt equal to zero, and negative discharges start and stop before the zero crossing.

Despite some differences being evident in the PRPD patterns of the AC and DCP cases that are strictly related to the different waveforms, some similarities are noteworthy. In particular, the detected PD pulse characteristics under AC stress, reported in Figures 7 and 8, are almost the same as those found with the DCP stress. In Figure 10, an acquired PD pulse under DCP stress is shown. The time domain response is identical to that under AC stress as well as the frequency spectrum. This confirms that the PD pulse characteristics are more related to the geometry of the defect than to the type of applied stress [23], [24].

Subsequently, by varying the parameter δ of the DCP waveform, the PRPD patterns have been obtained. Considering their similarity with those of the previous work, here only the PD features, summarized in Tables 2 and 3, are reported. As can be seen in [21], the more δ increases, the more the width of the spectrum $\Delta\Phi$ decreases, as well as the number of discharge pulses. Then, the DCP waveform with negative polarity has been applied as voltage stress and the resulting PRDP patterns for δ equal to 0 and 0.6 are shown in Figure 11. For $\delta = 0.8$, a very low number of PDs have been detected, whereas for $\delta = 1$, no PD events have been measured.

The differences in the pattern shape, between the tests with positive and negative polarity are mainly due to the different dielectric properties of the radiating surface. Under positive polarity, the electrons are provided by the electrode–air interface, whereas under negative polarity, the electrons are provided by

Table 2. Kapton specimen: Partial discharge (PD) features detected under AC and direct current periodic (DCP) test for positive and negative polarity for different values of δ[1]

	PDIV-DCP peak (kV)		PPS-DCP (PD/second)			
δ	+	−	+	−	PDIV-AC peak (kV)	PPS-AC (PD/second)
0.0	2.8	2.4	38	55	1.4	140
0.2	3.4	3.0	22	32		
0.4	4.2	3.9	16	23		
0.6	6.1	6.0	10	12		
0.8	10	8.3	2	3		
1.0[2]	14.28	11.46	0.4	0.8		

[1]PDIV = partial discharge inception voltage; PPS = pulse per second.
[2]Solutions of polynomial equations for $\delta = 1$.

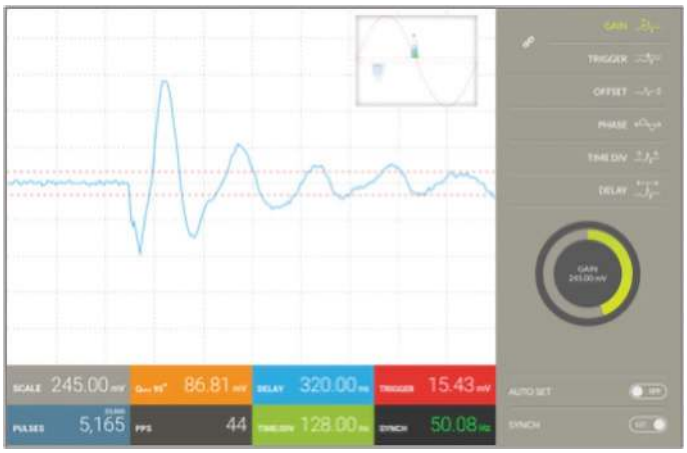

Figure 10. Negative partial discharge pulse detected under direct current periodic stress with $\delta = 0$.

Table 3. XLPE specimen: Partial discharge (PD) features detected under AC and direct current periodic (DCP) test for positive and negative polarity for different values of δ[1]

	PDIV-DCP peak (kV)		PPS-DCP (PD/second)			
δ	+	−	+	−	PDIV-AC peak (kV)	PPS-AC (PD/second)
0.0	2.2	1.9	15	20	1.6	60
0.2	2.9	3.0	5	15		
0.4	3.1	3.5	5	5		
0.6	4.7	5.1	5	2		
0.8	8.5	8.5	2	2		
1.0[2]	12.40	11.84				

[1]PDIV = partial discharge inception voltage; PPS = pulse per second.
[2]Solutions of polynomial equations for $\delta = 1$.

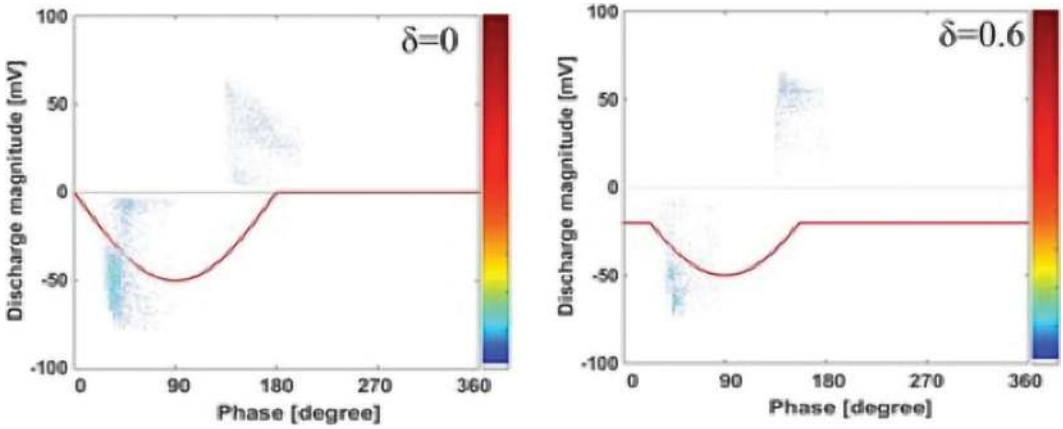

Figure 11. Phase-resolved partial discharge pattern acquired under the negative direct current periodic waveform, for δ values 0 and 0.6, in the Kapton specimen.

the air–Kapton interface. Under negative polarity it is also possible to notice that a certain amount of discharges is present in the constant part of the applied waveform. This phenomenon could be interpreted as analogous to what is termed "echo PD," which is explained in detail in [25], [26].

Regardless of the voltage polarity, it can be observed that when δ increases, the sinusoidal part of the DCP waveform decreases as well as dv/dt. This mainly causes a decrease of the PDRR and a reduction of the width of the spectrum $\Delta\Phi$ for both polarity discharges. In addition, when δ increases, the DCP looks more and more like the DC shape; therefore, the PDIV increases. Under AC and DCP waveforms, the detected PDIV (peak values) and PDRR, also referred to with the acronym PPS (pulse per second), are summarized in Table 2 with different δ values for positive and negative polarity.

It can be noted that the PDIV almost doubles from AC to DCP with $\delta = 0$ and, at the same time, the PPS decreases by about one third. The complete correlation between the PDIV and the parameter δ of the DCP waveform is shown in Figure 12, which also contains the second order polynomial fits to the experimental results of PDIV versus δ under positive and negative DCP stress.

The following polynomial formulae are the simplest mathematical expressions that fit to experimental data:

$$PDIV_{+} = 13.75\delta^2 - 2.45\delta + 2.98, \quad (6)$$

$$PDIV_{-} = 8.21\delta^2 + 0.83\delta + 2.42, \quad (7)$$

where the correlation coefficients R^2 are equal to 0.99.

The parabolic trend of the curve is useful for determining the variation in the value of PDIV under DC. This is because for δ greater than 0.8, the PDIV is greater than 10 kV, which is the maximum voltage level provided by the amplifier used in our measurement setup. This result is in line with what was previously achieved in [21]. As it can be observed, in both cases, the PDIV at constant DC voltage (DCP with $\delta = 1$) is approximately 14 kV. For the other values of δ, the offset between the two curves is very small. It is likely that this difference is due to the different acquisition systems used in the two studies, namely Pry-Cam prototype previously and portable Pry-Cam in the present paper.

The experimental results under DCP negative polarity show substantially the same trend as that under positive polarity, although the PDIV in the former case tends to be 2.8 kV lower than in the latter.

For Kapton, the PPS values also follow a second order polynomial trend. The findings of this case are reported in Table 2.

XLPE

The second material to be tested was XLPE, which is widely used in cable applications. Its structure provides pronounced resistance to abrasion, stress, chemicals, and temperature. In addition, because XLPE does not contain chloride, like PVC, it is more environmentally friendly. The same study and experi-

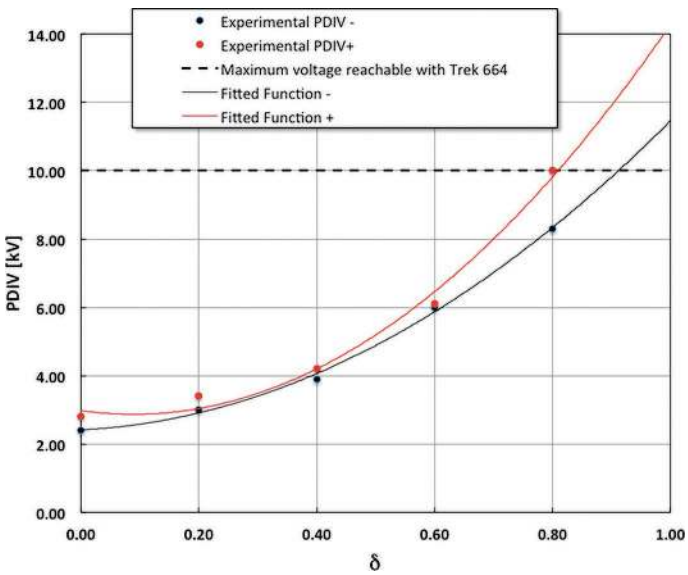

Figure 12. Experimental partial discharge inception voltage (PDIV) versus δ for the Kapton specimen for positive polarity (red circles) and negative polarity (black circles) and the second order polynomials in δ fitted to the experimental data (solid red and black lines).

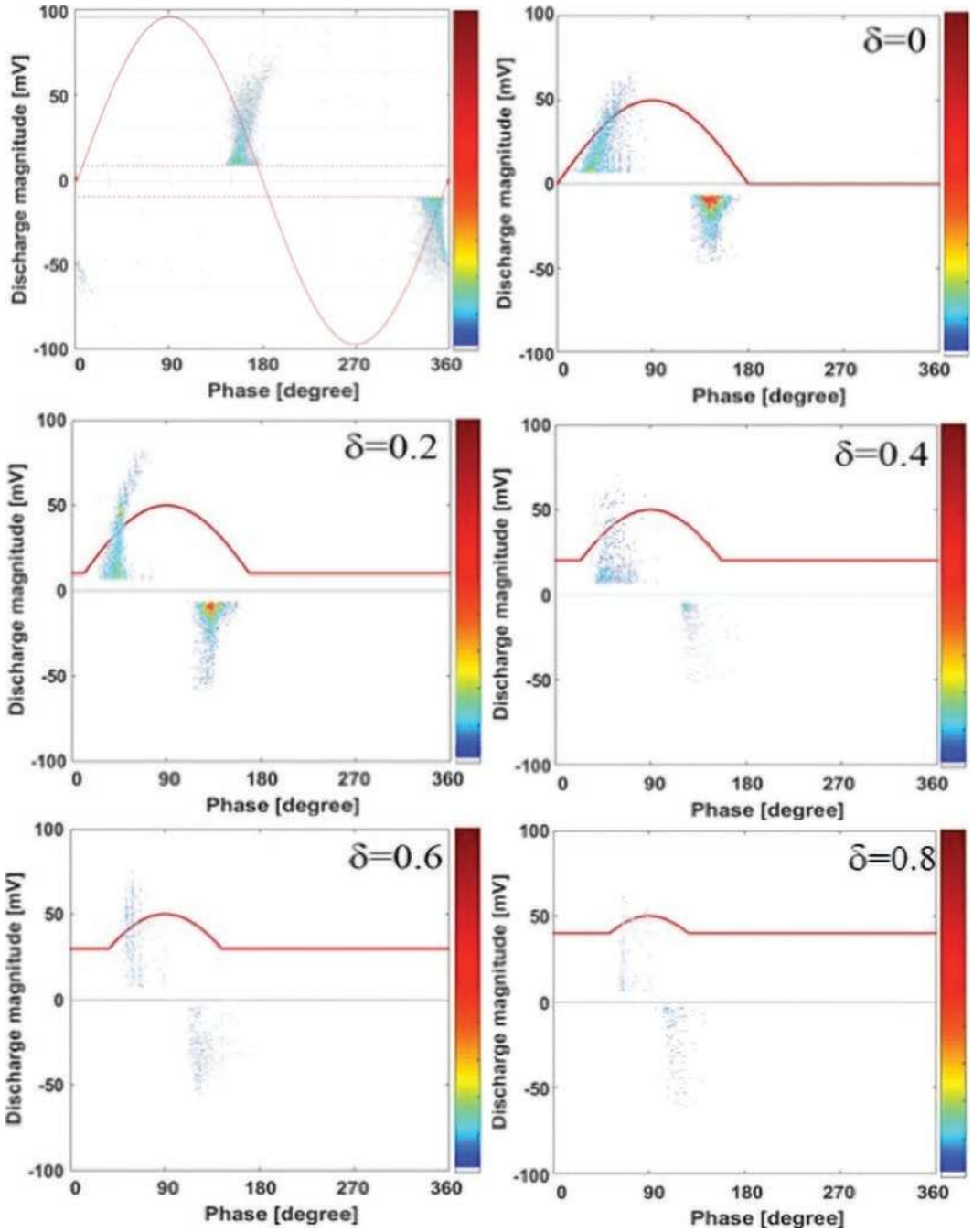

Figure 13. Phase-resolved partial discharge patterns acquired under AC and positive direct current periodic waveforms, for different values of δ, in the cross-linked polyethylene (XLPE) specimen.

mental tests, made for the Kapton specimen, were performed for the XLPE sample. The acquired AC and DCP PRPD patterns for positive polarity, and DCP PRPD patterns for negative polarity, are reported in Figures 13 and 14, respectively. In these figures, the voltage waveform is used only as a reference for the discharge phase, whereas the voltage values and the corresponding PPS are reported in Table 3. Contrary to what was observed in the Kapton specimen, in this case, for AC voltages and for low values of δ, the traditional "rabbit ear" of internal PDs is visible. This phenomenon is evident above all for the positive discharges, where the discharges are extinguished naturally as the dv/dt decreases both in AC and in DCP. A different behavior can be observed with negative discharges. In the AC case, negative discharges occur near the zero crossing of the voltage and show the same "rabbit ear" behavior as in the positive one. In the DCP case, negative discharges stop at a phase angle of $\pi - \alpha$, when the waveform transits from sinusoidal to constant shape. The differences in the pattern shape of the two specimens, Kapton and XLPE, are mainly due to the different dielectric material properties.

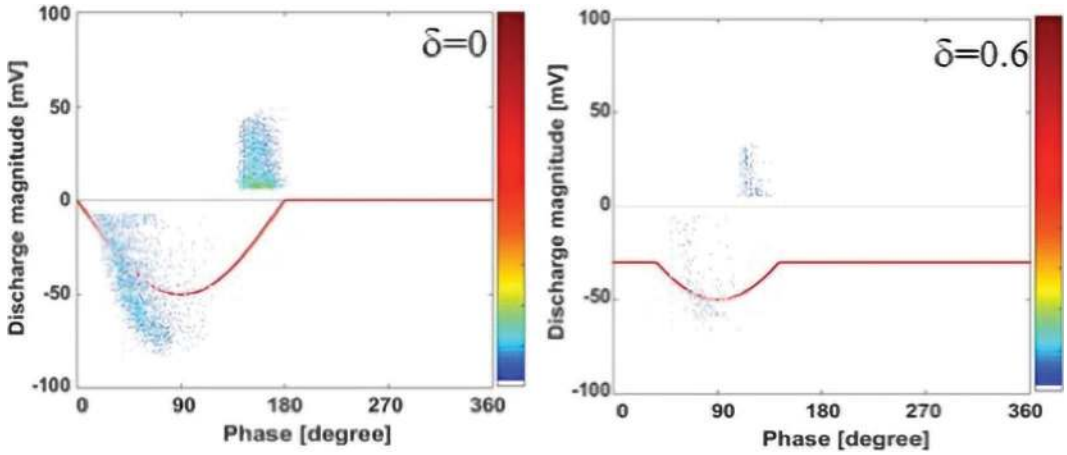

Figure 14. Phase-resolved partial discharge patterns acquired under the negative direct current periodic waveform, for different values of δ, in the cross-linked polyethylene (XLPE) specimen.

The negative DCP patterns show a behavior similar to that of positive ones. The most significant acquired patterns are reported in Figure 14.

The features of the acquired PDs, under positive and negative polarity of the DCP waveform, are summarized in Table 3. By comparing with the results found for the Kapton specimen, it can be noted that under AC, while the PDIV are almost the same, the PPS for the XLPE are less than 50% compared with Kapton. This highlights the XLPE's good resilience to partial discharges. Instead, δ-rated PDIV are on average lower than those of Kapton. Furthermore, unlike Kapton, no significant changes between the parameters detected for positive and negative polarity have occurred.

For XLPE material, the second order polynomial curves fitting PDIV results, plotted in Figure 15, are given by the following:

$$PDIV_{+} = 13.57\delta^2 - 3.66\delta + 2.49, \quad (8)$$

$$PDIV_{-} = 10.18\delta^2 - 0.49\delta + 2.15, \quad (9)$$

where the correlation coefficients R^2 are equal to 0.97.

As can be seen, for $\delta = 1$, the PDIV was not detected experimentally because it exceeds 10 kV. In this case, the solution of the polynomial equation in δ gives an estimated PDIV of approximately 12 kV, for both polarities. Unlike Kapton, however, in XLPE, the trend of the PPS does not follow a second order polynomial in δ. For this reason, Table 3 does not show DC trend values.

PET

The PET films, due to their excellent characteristics as an insulator, are usable in several electrical applications such as cable wrapping and motor insulation. The acquired AC and DCP PRPD patterns for positive and negative polarity are reported in Figures 16 and 17, respectively. Furthermore, in Table 4 the main features of the detected PD are summarized.

As can be seen in the obtained PRPD patterns, the "rabbit ear" shape is not visible, as for the Kapton sample. In addition, positive and negative parameters are very similar and often coincident.

The polynomial second order fitting curves, plotted in Figure 18, are given by

$$PDIV_{+} = 13.57\delta^2 - 3.45\delta + 2.39, \quad (10)$$

$$PDIV_{-} = 14.29\delta^2 - 3.83\delta + 2.40, \quad (11)$$

where the correlation coefficients R^2 are equal to 0.98.

Even for PET, for $\delta = 1$, the PDIV has not been detected experimentally because it exceeds 10 kV. In this case, the solution of the polynomial equation in δ gives an estimated PDIV of approximately 12.5 kV, for both polarities.

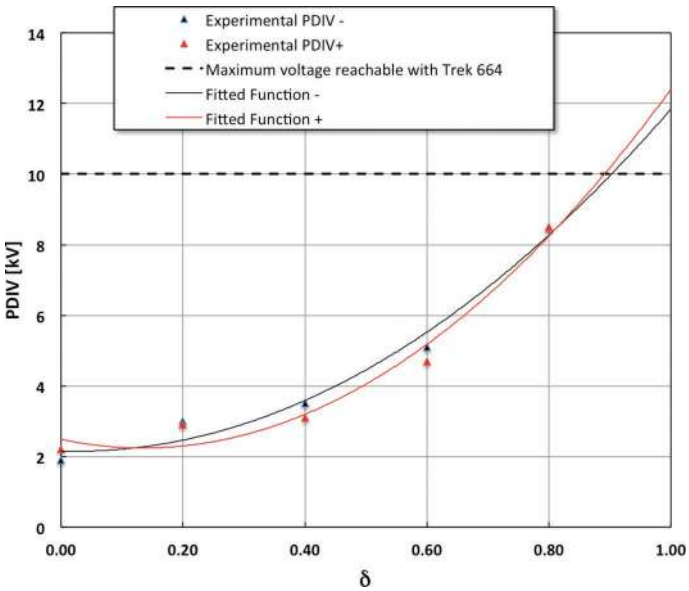

Figure 15. Experimental partial discharge inception voltage (PDIV) versus δ for the cross-linked polyethylene (XLPE) specimen for positive polarity (red triangles) and negative polarity (black triangles) and the second order polynomials in δ fitted to the experimental data (solid red and black lines).

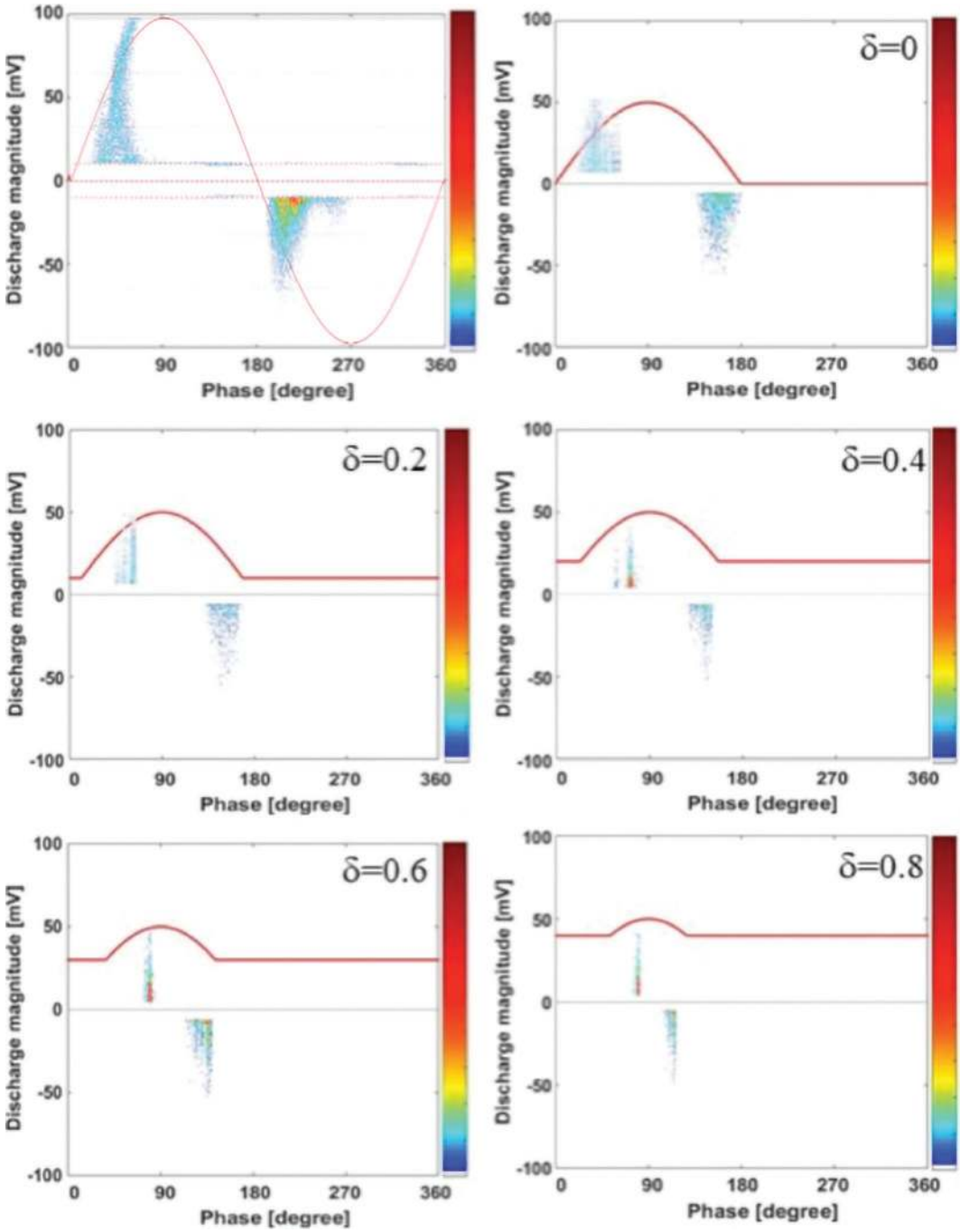

Figure 16. Phase-resolved partial discharge patterns acquired under AC and positive direct current periodic waveforms, for different values of δ, in the polyethylene terephthalate (PET) specimen.

Unlike Kapton and as with XLPE, PPS values do not follow a second order polynomial in δ. For this reason, Table 4 does not show DC trend values.

M.I. Paper

M.I. paper is one of the most common insulation materials in HVDC cables currently in service. The acquired AC and DCP PRPD patterns for positive polarity and DCP PRPD patterns for negative polarity are reported in Figures 19 and 20, respectively. In this case, due to the lower PDIV, experimental results have been also obtained for $\delta = 1$ for both polarities. In contrast to the other specimens, the M.I. paper PRPD pattern shows a strong reduction of double polarity discharges. Only with AC voltage does the PRPD pattern shows a classic "rabbit-like" behavior.

The polynomial second order fitting curves, plotted in Figure 21, are given by

$$\mathrm{PDIV}_{+} = 3.62\delta^2 + 1.51\delta + 2.57, \tag{12}$$

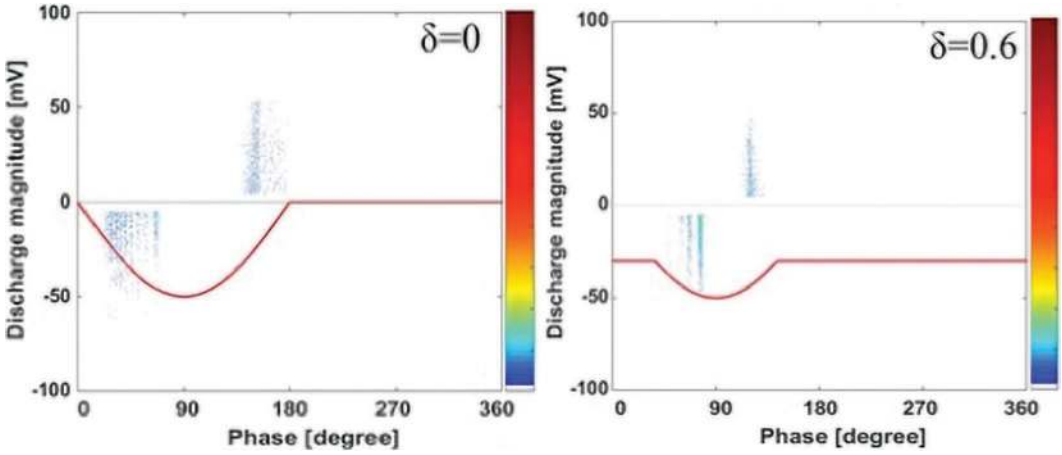

Figure 17. Phase-resolved partial discharge pattern acquired under the negative direct current periodic waveform, for different values of δ, in the polyethylene terephthalate (PET) specimen.

$$PDIV_{-} = 3.13\delta^2 + 1.75\delta + 2.80, \quad (13)$$

where the correlation coefficients R^2 are equal to 0.99.

In this case, all points are deduced experimentally, thus confirming the reliability of the polynomial approximation.

In Table 5 the main features of the detected PD are summarized.

However, these results have been obtained with difficulty, because more than once the M.I. paper specimens, despite the additional layer, have undergone breakdown during the test, such that it was necessary to replace them.

The M.I. paper shows a behavior similar to that of the other materials tested herewith but with some differences. The discharge phenomenon in AC has the typical behavior due to an internal void. The trend of PD pulses in the time and the frequency domain is almost superimposed on that of other materials. Conversely, by applying DCP, no discharges with double polarity have been detected. This phenomenon has been confirmed under negative polarity where only negative discharges appear. This is probably due to the very low PPS rate. Increasing the voltage, this phenomenon disappears and discharges of both polarities appear again. Moreover, this has been the only case with the pattern acquired for $\delta = 1$ (DC) and also in this case PD pulses have maintained the same shape and frequency content as the previous cases. The PD polarity has been determined by both the acquired pattern and the time domain response.

Table 4. Polyethylene terephthalate (PET): Partial discharge (PD) features detected under AC and direct current periodic (DCP) test for positive and negative polarity for different values of δ[1]

	PDIV-DCP peak (kV)		PPS-DCP (PD/second)			
δ	+	–	+	–	PDIV-AC peak (kV)	PPS-AC (PD/second)
0.0	2.2	2.2	16	16	1.4	60
0.2	2.6	2.6	14	11		
0.4	3.2	3.2	14	10		
0.6	4.8	4.8	8	10		
0.8	8.5	8.7	6	7		
1.0[2]	12.51	12.86				

[1]PDIV = partial discharge inception voltage; PPS = pulse per second.
[2]Solutions of polynomial equations for $\delta = 1$.

Discussions

To compare the results for all materials, it is however necessary to consider some dimensional differences shown in Table 1. With differences in thickness of the layers and of the cavities, the results in terms of the PDIV trend are not directly compa-

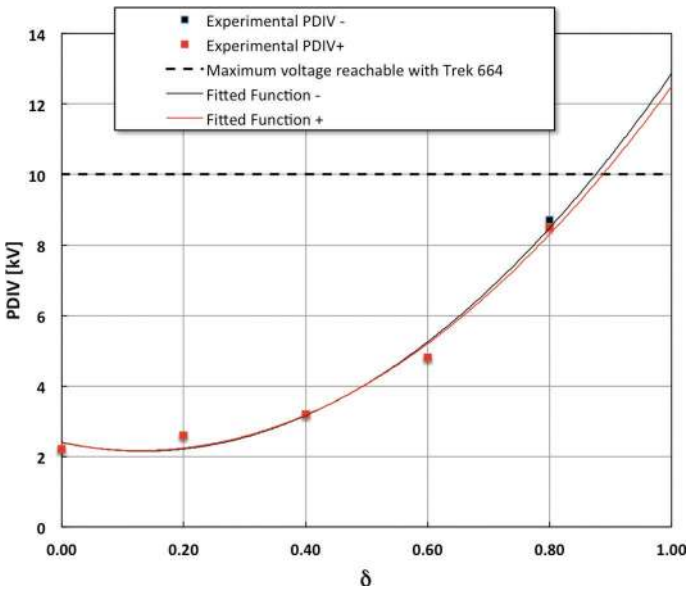

Figure 18. Experimental partial discharge inception voltage (PDIV) versus δ for the polyethylene terephthalate (PET) specimen for positive polarity (red squares) and negative polarity (black squares) and the second order polynomials in δ fitted to the experimental data (solid red and black lines).

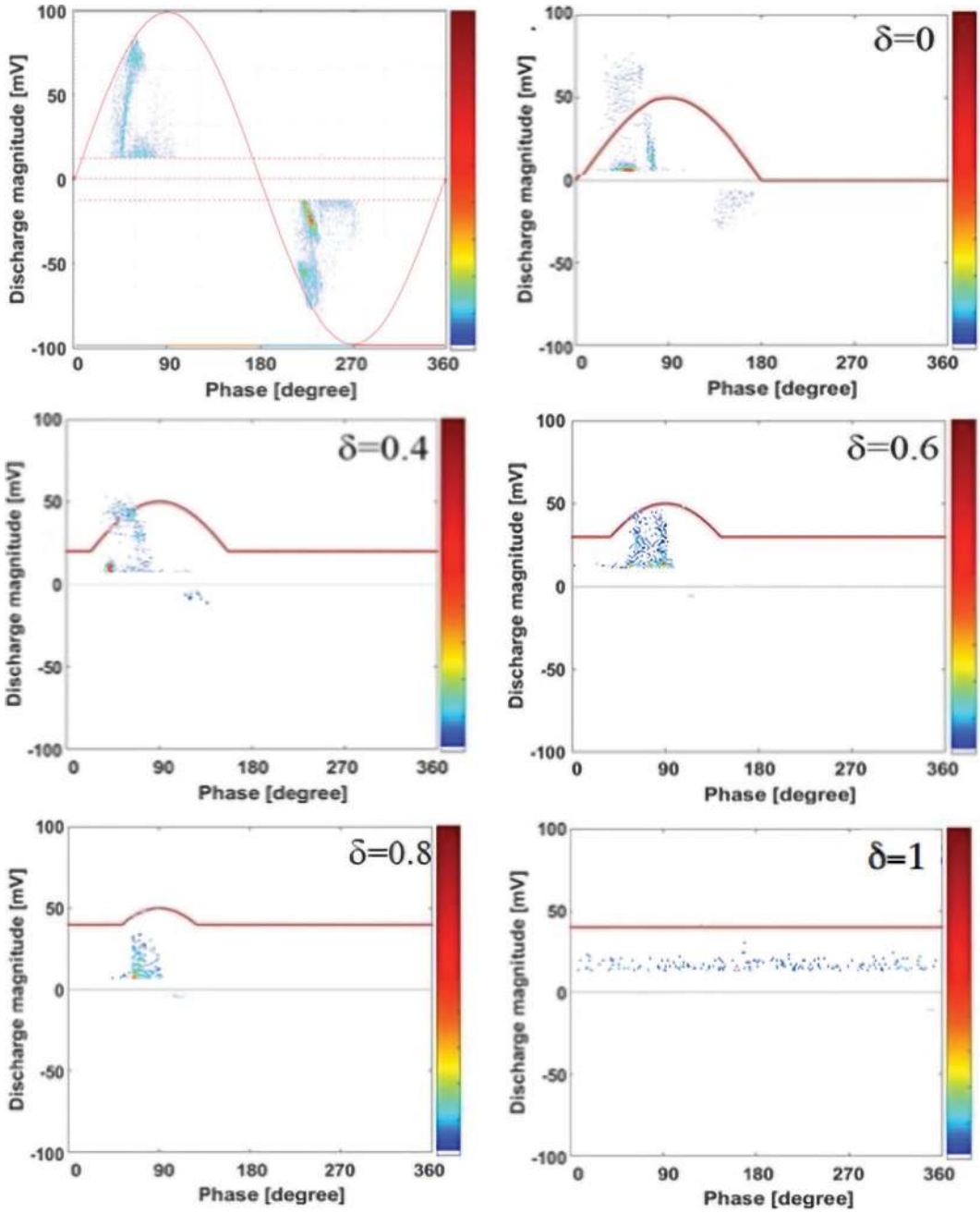

Figure 19. Phase-resolved partial discharge patterns acquired under AC and positive direct current periodic waveforms, for different values of δ, in the mineral oil mass impregnated (M.I.) paper specimen.

rable. Therefore, to compare the results, the value of the electric field applied inside the cavities has been determined. To do this, knowing the external PDIV, the voltage applied to the cavity boundaries has been calculated, through the simplified circuit models, both in AC (capacitive model) and in DC (ohmic-capacitive model) for DCP [27], [28]. The obtained results are shown in Figures 22 and 23. As is shown in Figure 22, for all the tested materials, the electric field depends on δ following a second order polynomial with an R^2 confidence of 0.97 to 0.99.

Kapton and PET exhibit very similar behavior, whereas XLPE, above $\delta = 0.4$, differs from the other polymeric materials because the value of the electric field grows faster than the others. At the same time, the M.I. paper has a flatter pattern with a lower slope than the other materials.

In Figure 23, a comparison of the different materials is shown in terms of corresponding electric field at the inception voltages in AC and DCP with $\delta = 0$ for both polarities. In addition, $\delta = 1$ tendency values are also added to compare the

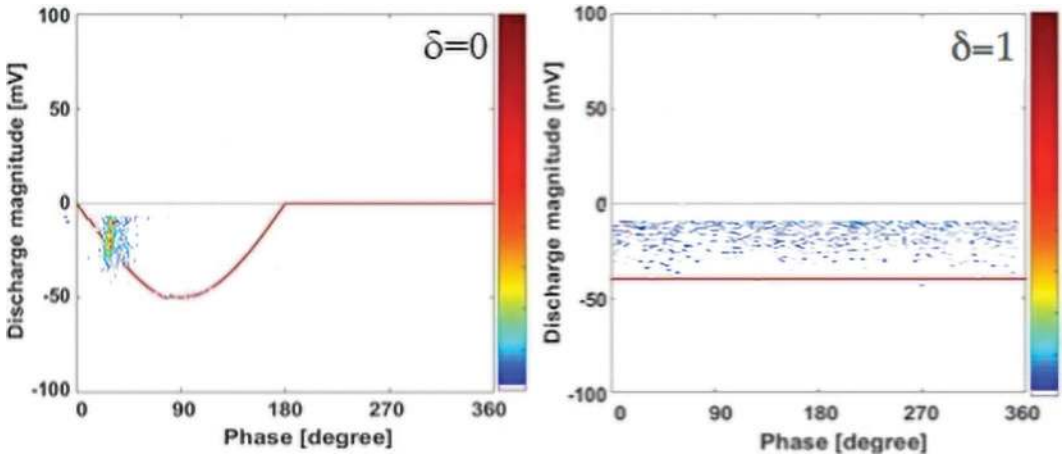

Figure 20. Phase-resolved partial discharge pattern acquired under the negative direct current periodic waveform, for different values of δ, in the mineral oil mass impregnated (M.I.) paper specimen.

experimental values obtained with the presumed DC values. First of all, the findings demonstrate a strong variation between inception electric field values under AC and DC. Again from this figure, it is evident that all materials have a similar behavior in terms of electric field values varying from AC to DC. With AC, values vary from 8 kV/mm for the Kapton to 13 kV/mm for the M.I. paper with a 60% variability. In DC, they vary from 85 kV/mm for the M.I. paper to 138 kV/mm for the XLPE, showing the same 60% variability. However, in this case, the XLPE and the M.I. paper have the maximum and the minimum value, respectively. The M.I. paper has the smallest variation between maximum and minimum value, whereas Kapton has the maximum. In terms of resilience to partial discharges, XLPE shows the best results.

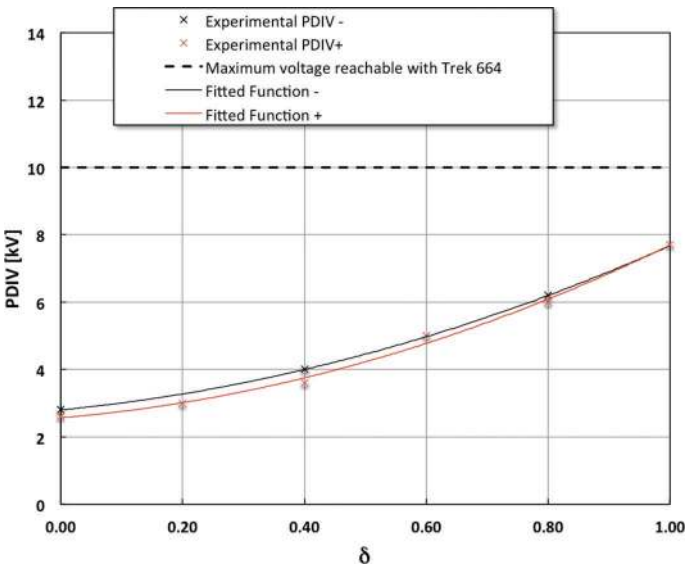

Figure 21. Experimental partial discharge inception voltage (PDIV) versus δ for the mineral oil mass impregnated (M.I.) paper specimen for positive polarity (red squares) and negative polarity (black squares) and the second order polynomials in δ fitted to the experimental data (solid red and black lines).

With reference to the obtained experimental data reported in the previous paragraphs, it can be noticed that, for all specimens, increasing the δ parameter causes an increase in the PDIV and a reduction of the PPS and the width of the spectrum, $\Delta\Phi_+$ and $\Delta\Phi_-$.

Conclusions

To overcome some issues related to the measurement of PD under DC stress, a new type of waveform has been developed as described in previous work. In that article, after introducing the DCP waveform, its performance has been verified in a Kapton sample and only in positive polarity. In this work, the DCP waveform under both polarities has been applied in another three dielectric samples: XLPE, PET, and M.I. paper. Beyond this, the Kapton sample has also been tested again to demonstrate the repeatability of the PD measured under DCP stress.

First of all, a numerical analysis demonstrates the similarity in terms of accumulated space charge at the interface between air and dielectric between DCP and DC. The similarities be-

Table 5. Mineral oil mass impregnated (M.I.) paper: Partial discharge (PD) features detected under AC and direct current periodic (DCP) test for positive and negative polarity for different values of δ[1]

	PDIV-DCP peak (kV)		PPS-DCP (PD/second)			
δ	+	–	+	–	PDIV-AC peak (kV)	PPS-AC (PD/second)
0.0	2.6	2.8	3	5	1.6	95
0.2	3.0	-	3	-		
0.4	3.6	4.0	2	2		
0.6	5.0	-	1	-		
0.8	6.0	6.2	1	1		
1.0	7.7	7.7				

[1]PDIV = partial discharge inception voltage; PPS = pulse per second.

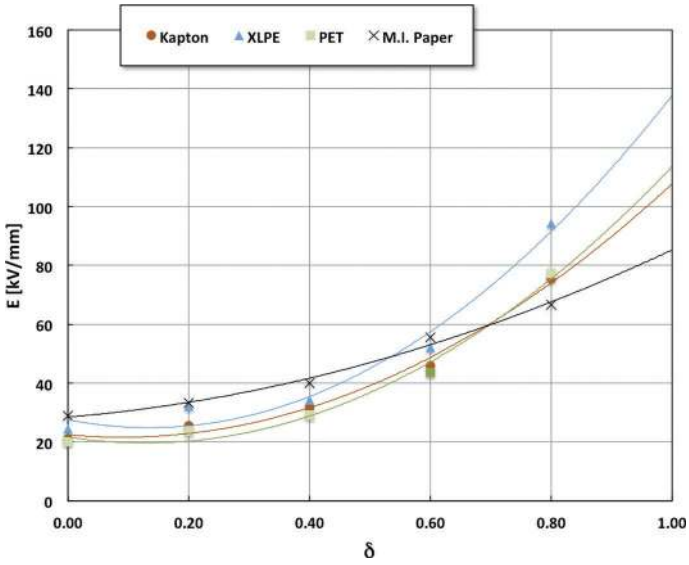

Figure 22. Comparison of the variation of electric field corresponding to the measured partial discharge inception voltage with δ and polynomial in δ fitted to the experimental data for positive polarity. XLPE = cross-linked polyethylene, PET = polyethylene terephthalate, and M.I. = mineral oil mass impregnated paper.

tween all the tested specimens have been experimentally confirmed in terms of PRPD patterns and PD responses in time and frequency domain.

For all the specimens, the recorded PDIV and PPS have been reported, as well as the most relevant PRPD patterns acquired under the DCP waveform with different δ values. The obtained results show that the Kapton's behavior detected in the previous work is confirmed also for the other materials and the PDIV depends on δ parameter as a second order polynomial. In terms of PPS, this trend is not confirmed in the same way. It is probably due to the reduced number of discharges detected at the

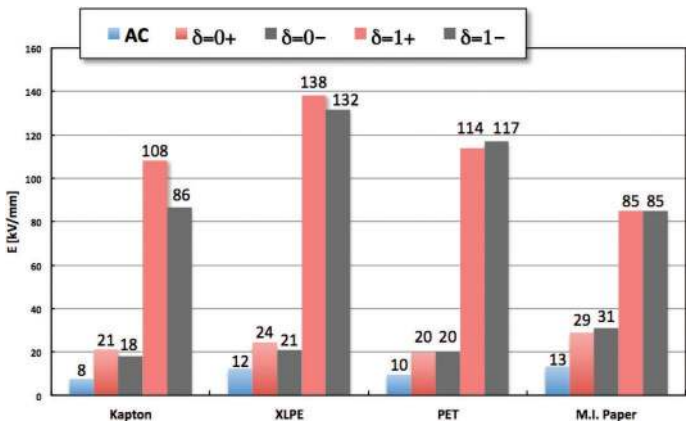

Figure 23. Comparison of the electric field corresponding to the measured partial discharge inception voltage in AC and with δ = 0 and the tendency with δ = 1 (DC) for positive and negative polarity. XLPE = cross-linked polyethylene, PET = polyethylene terephthalate, and M.I. = mineral oil mass impregnated paper.

inception voltages. Simultaneously, the width of the spectrum $\Delta\Phi_+$ and $\Delta\Phi_-$ and the phase distance between opposite polarity PD pulses are reduced. Similar results were obtained with negative polarity.

Due to the maximum voltage level of the measurement setup, the PDIV under the pure DC stress has been not experimentally detected but analytically predicted. However, considering geometrical differences among specimens, the corresponding electric field inside the cavities has been determined and a direct comparison has been performed. The results confirm a strong difference between experimental AC electric field, corresponding to internal PDIV, and that analytically predicted for a DC source. Moreover, XLPE shows the best results in term of resilience to the partial discharges.

In future work, these calculated PDIV values will be experimentally confirmed by adopting a suitable DC source with higher voltage level. Furthermore, PD measurements will be performed by applying DCP voltage supply for a long time to evaluate the effect of space charge accumulation at a different time from the beginning of the tests.

References

[1] G. Mazzanti and M. Marzinotto, "Improved design of HVDC extruded cable systems," in *Extruded Cables for High-Voltage Direct-Current Transmission: Advances in Research and Development*, 1, Wiley-IEEE Press, 2013.

[2] J. C. Fothergill, "The coming of age of HVDC extruded power cables," in *IEEE Electrical Insulation Conference (EIC)*, 2014, pp. 124–137.

[3] P. Morshuis, A. Cavallini, D. Fabiani, G. C. Montanari, and C. Azcarraga, "Stress conditions in HVDC equipment and routes to in service failure," *IEEE Trans. Dielectr. Electr. Insul.*, vol. 22, no. 1, pp. 81–91, 2015. https://doi.org/10.1109/TDEI.2014.004815.

[4] P. Romano, R. Candela, A. Imburgia, G. Presti, E. R. Sanseverino, and F. Viola, "A new technique for partial discharges measurement under DC periodic stress," in *IEEE Conf. on Electrical Insulation and Dielectric Phenomenon (CEIDP)*, 2017, pp. 303–306.

[5] *High-Voltage Test Techniques—Partial Discharge Measurements*, IEC 60270:2000+AMD1: 2015 CSV.

[6] P. Romano, A. Parastar, A. Imburgia, J. Blennow, M. Bongiorno, A. O. Di Tommaso, T. Hammarström, and Y. Serdyuk, "Partial discharge measurements under DC voltages containing harmonics produced by power electronic devices," in *IEEE Conf. Electrical Insulation and Dielectric Phenomena (CEIDP)*, 2018, pp. 558–561.

[7] A. Imburgia, P. Romano, F. Viola, N. Hozumi, and S. Morita, "Partial discharges behavior under different rectified waveforms," in *Int. Symp. Electrical Insulating Materials (ISEIM)*, 2017, pp. 114–117.

[8] U. Fromm, "Interpretation of partial discharges at DC voltages," *IEEE Trans. Dielectr. Electr. Insul.*, vol. 2, no. 5, pp. 761–770, 1995. https://doi.org/10.1109/94.469972.

[9] I. J. Seo, U. A. Khan, J. S. Hwang, J. G. Lee, and J. Y. Koo, "Identification of insulation defects based on chaotic analysis of partial discharge in HVDC superconducting cable," *IEEE Trans. Appl. Supercond.*, vol. 25, no. 3, pp. 1–5, 2015. https://doi.org/10.1109/TASC.2015.2394245.

[10] A. Pirker and U. Schichler, "Partial discharges at DC voltage—Measurement and pattern recognition," in *Int. Conf. Cond. Monit. Diagn. (CMD)*, 2016, pp. 287–290.

[11] H. Niu, A. Cavallini, G. Montanari, and Y. Zhang, "Noise rejection strategy and experimental research on partial discharge at DC voltage," in *IEEE 9th Int. Conf. Prop. Appl. Dielectr. Mater.*, 2009, pp. 489–492.

[12] M. A. Fard, A. J. Reid, and D. M. Hepburn, "Analysis of HVDC superimposed harmonic voltage effects on partial discharge behavior in solid dielectric media," *IEEE Trans. Dielectr. Electr. Insul.*, vol. 24, no. 1, pp. 7–16, 2017. https://doi.org/10.1109/TDEI.2016.005934.

[13] B. Qi, Z. Wei, and C. Li, "Creepage discharge of oil-pressboard Insulation in AC-DC composite field: phenomenon and characteristics," *IEEE Trans. Dielectr. Electr. Insul.*, vol. 23, no. 1, pp. 237–245, 2016. https://doi.org/10.1109/TDEI.2015.005404.

[14] W. Zhao, W. H. Siew, M. J. Given, E. Corr, Q. Li, and J. He, "Assessment of HDPE aged under DC voltage combined with AC harmonic stresses of various frequencies," *IEEE Trans. Dielectr. Electr. Insul.*, vol. 24, no. 2, pp. 1189–1196, 2017. https://doi.org/10.1109/TDEI.2017.006189.

[15] P. K. Olsen, F. Mauseth, and E. Ildstad, "The effect of DC superimposed AC voltage on partial discharges in dielectric bounded cavities," in *2014 ICHVE Int. Conf. High Voltage Engineering and Application*, 2014, pp. 1–4.

[16] M. A. Andrade, F. Burgio, R. Candela, L. De Rai, A. Imburgia, E. Riva Sanseverino, P. Romano, I. Troia, and F. Viola, "Partial discharge behavior under single phase half and full-bridge rectifier," in *IEEE Conference on Electrical Insulation and Dielectric Phenomenon (CEIDP)*, 2017, pp. 393–396.

[17] G. Mazzanti, J. Castellon, G. Chen, J. C. Fothergill, M. Fu, N. Hozumi, J. H. Lee, J. Li, M. Marzinotto, F. Mauseth, P. Morshuis, C. Reed, I. Troia, A. Tzimas, and K. Wu, "The insulation of HVDC extruded cable system joints. Part 1: Review of materials, design and testing procedures," *IEEE Trans. Dielectr. Electr. Insul.*, vol. 26, no. 3, pp. 964–972, 2019. https://doi.org/10.1109/TDEI.2019.8726046.

[18] G. Mazzanti, J. Castellon, G. Chen, J. C. Fothergill, M. Fu, N. Hozumi, J. H. Lee, J. Li, M. Marzinotto, F. Mauseth, P. Morshuis, C. Reed, I. Troia, A. Tzimas, and K. Wu, "The insulation of HVDC extruded cable system joints. Part 2: Proposal of a new AC voltage PD measurement protocol for quality control during routine tests," *IEEE Trans. Dielectr. Electr. Insul.*, vol. 26, no. 3, pp. 973–980, 2019. https://doi.org/10.1109/TDEI.2019.8726047.

[19] CIGRE Working Group B1.32. Recommendations for Testing DC Extruded Cable Systems for Power Transmission at a Rated Voltage up to 500 kV. CIGRE Technical Brochure 496. Paris, France: CIGRE, Apr. 2012.

[20] *Power Cables with Extruded Insulation and Their Accessories for Rated Voltages Above 150 kV (Um 1/4 170 kV) up to 500 kV (Um 1/4 550 kV) Test Method and Requirements*, 2nd ed., IEC 62067, Nov. 2011.

[21] P. Romano, G. Presti, A. Imburgia, and R. Candela, "A new approach to partial discharge detection under DC voltage," *IEEE Elec. Insul. Mag.*, vol. 34, no. 4, pp. 32–41, 2018. https://doi.org/10.1109/MEI.2018.8430041.

[22] M. A. Fard, M. E. Farrag, S. G. McMeekin, and A. J. Reid, "Partial discharge behavior under operational and anomalous conditions in HVDC systems," *IEEE Trans. Dielectr. Electr. Insul.*, vol. 24, no. 3, pp. 1494–1502, 2017. https://doi.org/10.1109/TDEI.2017.006469.

[23] P. Romano, A. Imburgia, and G. Ala, "Partial discharge detection using a spherical electromagnetic sensor," *Sensors (Basel)*, vol. 19, no. 5, p. 1014, 2019. https://doi.org/10.3390/s19051014.

[24] P. Romano, T. Hammarstrom, T. Bengtsson, A. Imburgia, A. Madonia, F. Viola, and S. M. Gubanski, "Partial discharges at different voltage waveshapes: Comparison between two different acquisition systems," *IEEE Trans. Dielectr. Electr. Insul.*, vol. 25, no. 2, pp. 584–593, 2018. https://doi.org/10.1109/TDEI.2018.006782.

[25] M. Florkowski, B. Florkowska, and P. Zydron, "Partial discharge echo obtained by chopped sequence," *IEEE Trans. Dielectr. Electr. Insul.*, vol. 23, no. 3, pp. 1294–1302, 2016. https://doi.org/10.1109/TDEI.2015.005487.

[26] M. Florkowski, B. Florkowska, and R. Włodek, "Investigations on post partial discharge charge decay in void using chopped sequence," *IEEE Trans. Dielectr. Electr. Insul.*, vol. 24, no. 6, pp. 3831–3838, 2017. https://doi.org/10.1109/TDEI.2017.006625.

[27] C. Pan, G. Chen, J. Tang, and K. Wu, "Numerical modeling of partial discharges in a solid dielectric-bounded cavity: A review," *IEEE Trans. Dielectr. Electr. Insul.*, vol. 26, no. 3, pp. 981–1000, 2019. https://doi.org/10.1109/TDEI.2019.8726048.

[28] G. Ala, R. Candela, P. Romano, and F. Viola, "Simplified hybrid PD model in voids," in *8th IEEE Symp. Diagnostics for Electrical Machines, Power Electronics and Drives*, 2011, pp. 451–455.

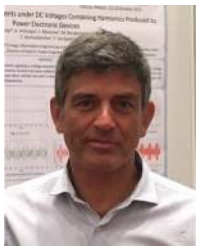

Pietro Romano (SM'17) received the MSc and PhD degrees in electrical engineering from the University of Palermo, Italy, in 1993 and 1998, respectively. From 1998 to 2001 he worked at CRES (Centre of Electronic Research in Sicily) on partial discharge measurement research. Since 2001 he has been a researcher in the DEIM Department of the University of Palermo, and he teaches Basic Electrical Engineering, Electrotechnics and Insulating Materials. His research activity is mainly in the fields of insulating systems diagnosis, partial discharge and space charge measurements, HV systems, multifactor stress effects, and electric field simulations. He is the head of the L.E.PR.E. HV Laboratory of Palermo University.

Antonino Imburgia was born on April 28, 1987, in Palermo, Italy. He received the MSc degree in electrical engineering from the University of Palermo, Palermo, Italy, in 2014. Since 2015 he has been working as a PhD and as a researcher with the Department of Engineering, University of Palermo. His research interests include HVDC, distribution of space charge in solid dielectrics and its behavior, dielectrics and electrical insulating systems diagnosis, space charge and partial discharge measurements.

Giuseppe Rizzo (S'19) is a graduate student member of IEEE. He received his master's degree in nuclear engineering from the University of Palermo in 2008. After a brief time at the Nuclear Engineering Department of the University of Palermo, from 2009 to 2018, he worked as a researcher and designer of small wind turbine generators at Jonica Impianti. Since 2018 he has been a PhD student in the

Engineering Department of the University of Palermo working on a research project at the L.E.PR.E. HV Laboratory on space charge measurements by means of the PEA method.

Guido Ala (SM'16) was born in 1964. He received the "Laurea" degree (MD) in electrical engineering from the University of Palermo, Palermo, Italy, and the PhD degree in electrical engineering from Italian MIUR, Rome, Italy, in 1989 and 1994, respectively. From 1992 to 1996 he was a teacher (permanent staff) of electrothecnics with the Italian Technical High Schools. In 1997 he was an energy engineer with the Municipal Gas Company, Palermo, Italy. From 1997 to 2004 he was a researcher with the University of Palermo, where he has been an associate professor with the Department of Engineering since 2005. In 2017 he attained the National Scientific Qualification for the role of a full professor in electrical engineering. His research interests include computational electromagnetics, grounding systems, lightning, electromagnetic compatibility, partial discharge detection, bio-electromagnetic numerical modeling, and electrical analogies in viscoelasticity.

Roberto Candela has conducted research since 1995 in the field of partial discharges in the dielectric laboratory of the University of Palermo, with particular focus on the development of equipment and software aimed at the analysis and measurement of partial discharges in solid insulation. From 2001 to 2011 he was a researcher at the Department DEIM at the University of Palermo, and he taught electrotechnics and insulating materials. Since 2012 he has been CEO of Prysmian Electronics, part of Prysmian Group.